JOURNAL OF APPLIED ELECTROCHEMISTRY 9 (1979) 291–299

Potential distribution model for rechargeable sulphur electrodes in sodium–sulphur cells

M. W. BREITER, B. DUNN

General Electric Company, Corporate Research and Development, Schenectady, NY 12 301, USA

Received 13 March 1979

The efficiency of laboratory type sodium–sulphur cells, especially the utilization of reactants, is critically dependent upon the design of the sulphur electrode. The satisfactory rechargeability of a new design, based on a graduated electronic resistance inside the carbon fibre matrix is analysed in terms of two models: (a) predominant influence of potential distribution, (b) predominant influence of free flow in open spaces. Experimental results in favour of model (a) are discussed. The potential distribution of the new design is computed using appropriate assumptions for the one-phase region and compared with that in the absence of a graduated electronic resistance. It appears that the improved rechargeability can be explained by the different potential distribution.

1. Introduction

The results reported by the various groups engaged in sodium–sulphur cell testing [1–5] clearly indicate that the rechargeability and, therefore, the utilization of reactants critically depends upon the design of the sulphur electrode. Whereas the discharge of sodium–sulphur cells can be accomplished easily, a satisfactory charge is only feasible for cells with an appropriately constructed sulphur electrode. In poorly constructed devices the cell voltage during charge becomes relatively large as the end of the one-phase region is approached. Conversion of lower polysulphides to Na_2S_5 occurs but operation in the two-phase region (i.e., where Na_2S_5 is further converted to sulphur) is severely inhibited. Thus, cells with inadequate sulphur electrode design can only be cycled in the one-phase region and less than 50% of the reactants are utilized. Such poor cycling behaviour is usually apparent during the first cycle.

In this paper experimental studies and theoretical considerations are presented for a new sulphur electrode design which consistently permits sodium–sulphur cells to be charged into the two-phase region [2, 6]. A model for rechargeability is derived based on the spatial distribution of carbon mat and polysulphide potentials within the electrode. Experimental evidence favours this approach over an alternate one involving mass transport of reactants and products in open spaces [4, 7]. The potential distribution model also indicates some measure of the electrochemical reactions occurring at the carbon/sodium polysulphide interfaces. This information suggests certain processes which are liable to affect long-term cell performance, i.e., a gradual loss of cell capacity accompanied by an increase in cell resistance. Although it is likely that more than one factor is responsible for these effects [1, 4, 5], the proposed model illustrates how the sulphur electrode is apt to contribute.

2. Experimental distinction between potential distribution and mass transport processes in open spaces

Two sulphur electrode configurations allowed the sodium–sulphur cell to charge into the two-phase region (Fig. 1). In the early design (Fig. 1a) a cylindrical carbon fibre/sulphur plug was produced by stuffing Thornel carbon fibre mat VM0032 into a Teflon polymer mould and pouring in the required amount of sulphur. A centre hole for the beta-alumina tube was drilled. Subsequently, either four or six small holes were drilled parallel to the centre bore in a symmetrical fashion. During cell assembly, the space between

the walls of the centre bore and the beta-alumina tube was stuffed with carbon fibres, initially Thornel carbon fibre mat VM0034 and later VM0031 (designated as mats 34 and 31 respectively).

The mass transport model [4] suggests that the free flow of reactants and products in open spaces is responsible for operation in the two-phase region and that the creation of open space enhances this process. However, in experiments where the symmetrical holes were filled with glass rods (i.e., extremely limited flow) cell behaviour was unaffected. That is, cells cycled into the two-phase region regardless of the presence or absence of glass rods in the holes. Clearly, a reason other than free flow in open spaces is responsible for the improved rechargeability. This conclusion is supported by the additional observation that in failed or discontinued cells the holes (without glass rods) did not contain sulphur or polysulphide when disassembled.

The preceding conclusion is confirmed by the results of cycling cells with the latest sulphur electrode design (Fig. 1b). This design does not incorporate any free spaces. The solid carbon fibre/sulphur plug is prepared in the same fashion and after drilling the centre bore it is cut into two halves. Two thin, equal sized segments of mat 32 are placed adjacent to the surface of the inner bore. Two identical strips of another mat with larger resistance are put inside the sections of mat 32. The two halves then encircle the beta-alumina tube and the cell is assembled. Cells of this design are easier to manufacture, require no drilling of small holes and cycle well into the two-phase region.

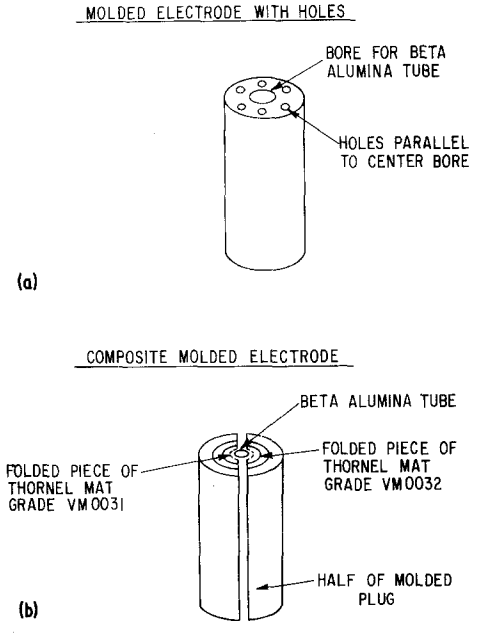

Fig. 1. Moulded sulphur electrode with graded resistance. (a) Early design with drilled holes; (b) later design using layers of carbon mat.

The improvement in rechargeability is attributed to a gradient of the electronic resistance inside the sulphur electrode. The model derived in subsequent sections indicates that the resistance increase towards the centre prevents sulphur deposition from occurring at the beta-alumina surface during charging. Experimental results on laboratory cells support this hypothesis.

3. Experimental determination of carbon mat resistivities in the sulphur electrode

The potential distribution model presented in this paper requires resistivity values for the various carbon mats. Mat resistance and, therefore, cell behaviour are extremely sensitive to the degree of mat compression (i.e., its bulk density) [8]. Thus, measurements must be made under simulated operating conditions to minimize the possibilities of error.

A cell closely resembling the sulphur electrode was constructed and tested (Fig. 2). The high sulphur resistivity ensured that conduction through the carbon/sulphur plug would be electronic (via carbon fibres). A graphite rod replaced the usual beta-alumina electrolyte and served as the counter electrode. Mat 32/sulphur plugs were fabricated in the usual fashion and the thin mat layers free of sulphur were wrapped normally. The resistance (at 1 kHz) was measured as a function of temperature.

Three configurations were evaluated; (a) mat 32/sulphur plug without any additional layers, (b) mat 32/sulphur plug with high resistance mats covering the counter electrode and (c) mat 32/sulphur plug with mat 32 covering the counter electrode. Condition (a) allows the mat 32 resistivity to be measured directly while (b) corresponds to the sulphur electrode geometry generally employed in cells. By comparing (c)

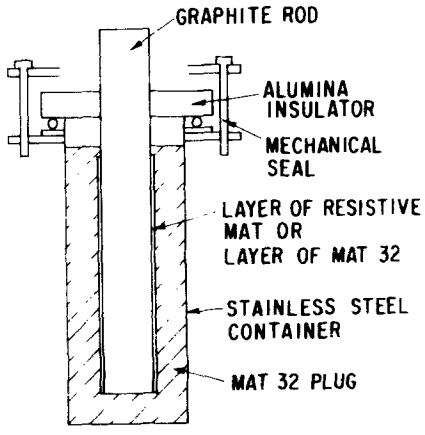

Fig. 2. Experimental arrangement for measuring carbon mat resistance.

with (a), one may determine whether a contact resistance exists between the sulphur impregnated and unsaturated mats. The results indicate that as the sulphur melts it improves the electrical contact within the system and lowers the resistance commensurately (Fig. 3). The temperature dependence of this transition depends upon the heating rate and perhaps the wetting characteristics of the originally unsaturated layer. Item (a) is not shown because it is identical to (c); i.e., there is no evidence of a contact resistance between mats.

Clearly the high resistance of case (b) resulted from the presence of the resistive carbon layers. Additional d.c. measurements were performed and only ohmic behaviour was observed. Agreement with the 1 kHz values was excellent. Resistances for cases (b) and (c) were 10 Ω and 0·070 Ω, respectively. Calculated values of resistivity were 3·88 Ω cm for mat 32 and 2725 Ω cm for the high resistance layer.

4. Potential distribution for the sulphur electrode with gradated electronic resistance

4.1. *Basic assumptions of model*

The three basic assumptions are identical to the ones used in the model derived previously by Gibson [3] for a sulphur electrode with constant electronic resistance (i.e., the homogeneous case).

4.1.1. Approximation (a). The potential distribution is computed for a linear and not a cylindrical geometry. This assumes that the only potential gradients are perpendicular to the major axis of the cell. In laboratory sodium–sulphur cells where the outer diameter of the beta-alumina tube approaches the thickness of the carbon fibre/sulphur plug (1 cm and 0·7 cm respectively) the model can only give an approximate solution. Nonetheless, it adequately describes the main features of the sulphur electrode with gradated resistance. This solution, however, becomes a much better representation for our full-sized cells where the outer diameter of the beta-alumina tube is roughly 2·5 cm and the carbon fibre/sulphur plug thickness remains at 0·7 cm.

4.1.2. Approximation (b). The potential distribution is derived for steady state conditions instead of a time-dependent approach. This

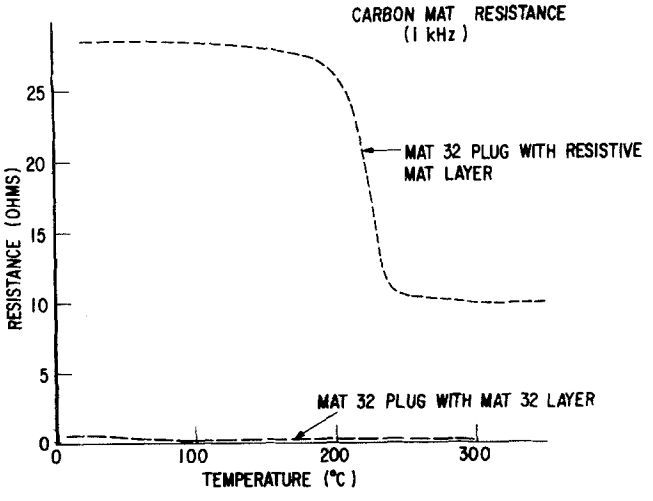

Fig. 3. Carbon mat resistance as a function of temperature.

restricts the validity of the solution to the one-phase region. The resistivity of the homogeneous melt does not change very much in this region during cycling and, therefore, average values can be used. Despite this restriction, the potential distribution yields important information concerning the probability of preferential sulphur deposition in the vicinity of the surface of the beta-alumina tube during charging.

4.1.3. Approximation (c). The simplifying assumption is made that the electrochemical reaction rate is proportional to the difference of inner potentials between the carbon fibre and melt. Judging from recent kinetic studies in polysulphide melts on solid carbon electrodes [9–12], the current–potential curves display a linear region in the vicinity of the reversible potential in a given melt. The linear region extends further than can be accounted for by linearizing the expression for the rate-determining process. A possible interpretation for such behaviour was advanced [10]. From a practical point of view it is sufficient to know that a linear relationship between current and electrode potential exists and serves as a good approximation for about 100 mV in the vicinity of the reversible potential in Na_2S_3 and Na_2S_4 melts.

4.2. *Derivation of potential distribution*

A schematic diagram of the linear model for the gradated resistance sulphur electrode is shown in Fig. 4 (compare with Fig. 1b). The x-axis for region 2 (mat 32) extends from the container wall to the mat 32/mat 31 interface (from $x = 0$ to $x = x_2$). Region 2 is characterized by the electronic resistance per unit length of mat 32 (r_2 in $\Omega\,cm^{-1}$), the melt resistance per unit length (R in $\Omega\,cm^{-1}$) and the slope resistance per unit volume of the current/voltage curve (ρ in Ω cm). R and ρ are considered to be independent of x and therefore assume the same values in region 1. In addition, this region possesses an electronic resistance $r_1 \gg r_2$ for mat 31. Its thickness, much less than region 2, extends between the mat 32/mat 31 interface and the surface of the beta-alumina (i.e., from $x = 0$ to $x = x_1$). The model is treated for unit cross-sectional area.

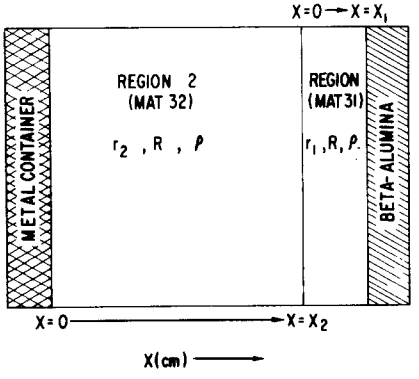

Fig. 4. Schematic of sulphur electrode used in the potential distribution model.

Using the same approach as Daniel-Beck [13] who represented a pore inside a porous electrode by a transmission line, the following equations hold for both regions:

$$\frac{d^2\phi_c}{dx^2} = -r\frac{dI}{dx} \tag{1}$$

$$\frac{d^2\phi_m}{dx^2} = -R\frac{dJ}{dx} \tag{2}$$

$$\frac{\phi_c - \phi_m}{\rho} = \frac{dI}{dx}\,. \tag{3}$$

Here ϕ_c and ϕ_m designate the inner potentials of the carbon fibre matrix and melt, respectively, while I and J are the electronic and ionic current fluxes through the carbon fibre matrix and melt respectively. Equation 3 represents the electrochemical reaction rate occurring within a small element of carbon felt. If a negligible formation of corrosion products is assumed to occur at the container wall, then at any point within the electrode

$$I + J = I_0\,. \tag{4}$$

The current, I_0, is that injected at the container wall. It follows from Equations 1–3 with the aid of Equation 4:

$$\frac{d^2(\phi_c - \phi_m)}{dx^2} + \frac{R+r}{\rho}(\phi_c - \phi_m) = 0. \tag{5}$$

The general solution of Equation 5 is

$$\phi_c - \phi_m = A\exp(k^{1/2}x) + B\exp(-k^{1/2}x) \tag{6}$$

with

$$k = \frac{R+r}{\rho}. \tag{7}$$

Since r has different values in region 1 and region 2, k will vary accordingly. The solutions of region 1 and 2 can be numerically evaluated after the respective integration constants (A_1 and B_1 for region 1, A_2 and B_2 for region 2) are determined from the boundary conditions. These conditions, previously described by Gibson [3] for the homogeneous case, are entirely applicable to the present model. At the container wall only electronic current exists and

$$\frac{d(\phi_c - \phi_m)}{dx} = \frac{d\phi_c}{dx} - \frac{d\phi_m}{dx} = -r_2 I_0. \quad (8)$$

At the beta-alumina surface the current is ionic

$$\frac{d(\phi_c - \phi_m)}{dx} = \frac{d\phi_c}{dx} - \frac{d\phi_m}{dx} = RI_0. \quad (9)$$

At the interface between mat 32 and mat 31 a general condition is employed; the potential distribution and its slope are continuous.

$$(\phi_c - \phi_m)_{\text{region 2}} = (\phi_c - \phi_m)_{\text{region 1}} = Y \quad (10)$$

$$\left[\frac{d(\phi_c - \phi_m)}{dx}\right]_{\text{region 2}} = \left[\frac{d(\phi_c - \phi_m)}{dx}\right]_{\text{region 1}}. \quad (11)$$

The latter boundary condition (Equation 11) is an approximation. Although the ionic current is continuous at the interface, the electronic resistivity changes. Nonetheless, the assumption is valid from both physical and analytical standpoints. The large resistance of mat 31 compels virtually all the current to be carried through the melt while the electronic phase, regardless of the discontinuity at the interface, contributes insignificantly to the total current. This same conclusion is reached by determining the ratio of electronic currents for each region, I_1/I_2. The continuity of $d\phi_m/dx$ at the interface implies that this ratio is equal to their resistances per unit length or 4/2500 in the present case (i.e., $\ll 1\%$). By using a more quantitative procedure, where the sulphur electrode is described by a resistor network, the I_1/I_2 value at the interface becomes 4/1254 (also $\ll 1\%$). For numerical purposes, it hardly matters whether 4/2500 or 4/1254 is chosen for I_1/I_2. These two approaches substantiate the assertion that the boundary condition (Equation 11) is a good approximation. It also enables a mathematical solution to be obtained directly.

Constants A_2 and B_2 are determined by using Equation 8 at $x = 0$ and Equation 10 at $x = x_2$. The simultaneous equations are subsequently solved in terms of Y.

$$A_2 = \left[Y - \frac{r_2 I_0}{k_2^{1/2}} \exp(-k_2^{1/2} x_2)\right] \exp(-k_2^{1/2} x_2) \quad (12)$$

$$B_2 = \left[Y + \frac{r_2 I_0}{k_2^{1/2}} \exp(k_2^{1/2} x_2)\right] \exp(-k_2^{1/2} x_2). \quad (13)$$

A similar approach is used to obtain A_1 and B_1. In this case Equation 10 is employed at $x = 0$ and Equation 9 at $x = x_1$.

$$A_1 = \left[Y \exp(-k_1^{1/2} x_1) + \frac{RI_0}{k_1^{1/2}}\right] \exp(-k_1^{1/2} x_1) \quad (14)$$

$$B_1 = \left[Y \exp(k_1^{1/2} x_1) - \frac{RI_0}{k_1^{1/2}}\right] \exp(-k_1^{1/2} x_1). \quad (15)$$

The only approximations used in deriving these equations are that $\exp(k_1^{1/2} x_1) \gg \exp(-k_1^{1/2} x_1)$ and $\exp(k_2^{1/2} x_2) \gg \exp(-k_2^{1/2} x_2)$. These conditions are easily satisfied for the sulphur electrodes of interest. The value of $(\phi_c - \phi_m)$ at the mat 31/mat 32 interface is obtained by using Equation 11 which for the two regions becomes

$$k_2^{1/2}[A_2 \exp(k_2^{1/2} x_2) - B_2 \exp(-k_2 x_2)] = k_1^{1/2}(A_1 - B_1). \quad (16)$$

Equations 12–15 are substituted and

$$Y = 2I_0 \left[\frac{R \exp(-k_1^{1/2} x_1) + r_2 \exp(-k_2^{1/2} x_2)}{k_2^{1/2} + k_1^{1/2}}\right]. \quad (17)$$

Equations for $(\phi_c - \phi_m)$ may now be developed. For our specific sulphur electrodes additional simplifications can be made. These are

$$\exp(-2k_2^{1/2} x_2) \gg \exp(-k_1^{1/2} x_1 - k_2^{1/2} x_2)$$

and

$$\exp(-k_2^{1/2} x_2) \gg \exp(-k_1^{1/2} x_1).$$

Substituting Equation 17 into Equations 14 and 15 enables $(\phi_c - \phi_m)$ to be determined for region 1 by using Equation 6

$$(\phi_c - \phi_m)_1 = \frac{RI_0}{k_1^{1/2}} \exp(-k_1^{1/2} x_1 + k_1^{1/2} x) +$$

$$+\frac{2I_0r_2}{k_1^{1/2}+k_2^{1/2}}\exp(-k_2^{1/2}x_2-k_1^{1/2}x). \quad (18)$$

Similarly, $(\phi_c-\phi_m)$ is obtained for region 2 by substituting Equation 17 into Equations 12 and 13 and using Equation 6

$$(\phi_c-\phi_m)_2 = r_2I_0\exp(-2k_2^{1/2}x_2+k_2^{1/2}x) \times\left[\frac{2}{k_1^{1/2}+k_2^{1/2}}-\frac{1}{k_2^{1/2}}\right]+\frac{r_2I_0}{k_2^{1/2}}\exp(-k_2^{1/2}x). \quad (19)$$

It is quite instructive to compare the solution obtained for the dual mat configuration (Fig. 4) with that of the single mat geometry. The latter is characterized by only one mat resistance, r_c, from the container wall ($x = 0$) to the solid electrolyte ($x = L$). A solution for this situation is obtained by the same procedure as the one outlined above with the appropriate boundary conditions (Equations 10 and 11) being eliminated. A and B in Equation 6 become

$$A = \frac{I_0[R_m+r_c\exp(-k^{1/2}L)]}{2k^{1/2}\sinh k^{1/2}L} \quad (20)$$

$$B = \frac{I_0[R_m+r_c\exp(k^{1/2}L)]}{2k^{1/2}\sinh k^{1/2}L}. \quad (21)$$

Substituting these into Equation 6, the single mat or homogeneous resistance case is obtained

$$\phi_c-\phi_m = \frac{I_0R\cosh k^{1/2}x+I_0r_c\cosh k^{1/2}(L-x)}{k^{1/2}\sinh k^{1/2}L}. \quad (22)$$

Gibson [3] solved the identical configuration by a slightly different procedure. Numerical solutions for the two approaches, however, result in nearly perfect agreement.

5. Discussion

The dual mat arrangement (Equations 18 and 19) was evaluated with the aid of computer programs using relevant parameters for the sulphur electrode. In the calculations $R = 4\,\Omega\,cm^{-1}$, $r_1 = 2500\,\Omega\,cm^{-1}$ and r_2 was varied ($r_2 = 0{\cdot}4$, $4{\cdot}0$, $20{\cdot}0\,\Omega\,cm^{-1}$). The thicknesses of regions 1 and 2 were 0·08 cm and 0·58 cm, respectively, and $I_0 = 0{\cdot}1$ A. For the single mat case $r = r_2$ and $L = x_1 + x_2 = 0{\cdot}66$ cm. Equation 7 was used to determine k, k_1 and k_2 by using the appropriate r value. The slope resistance, ρ, was previously chosen by Gibson [3] to be $0{\cdot}02\,\Omega$ cm. There is, however, some validity to this value if one considers the impedances reported by Armstrong *et al.* [10] at the equilibrium potential and in the linear region to be normalized to the appropriate surface area per unit volume.

Cell dimensions and the resistances for r_1 and $r_2 = 4\,\Omega\,cm^{-1}$ reflect actual cell values. The upward variation of r_2 is limited by the conditions used in deriving Equations 18 and 19. R corresponds reasonably well to Na_2S_4.

The results of the analysis are illustrated in Figs. 5–7. It is significant to note that $(\phi_c-\phi_m)$ provides information in two related areas; (a) it represents a quantity directly proportional to the electrochemical reaction rate, dI/dx (Equation 3), and (b) it may also be related to the electrochemical processes occurring at the carbon/sodium polysulphide interface. These two aspects are considered separately.

5.1. *Reaction rate distribution*

The reaction rate distribution is illustrated in Figs. 5–7 for both single and dual mat configurations. From Equation 3 it is apparent that in the regions where $(\phi_c-\phi_m)$ approaches zero the reaction rate diminishes accordingly while in the other area it is enhanced.

The zero value for $(\phi_c-\phi_m)$ is somewhat misleading. It arises from the use of the same ρ regard-

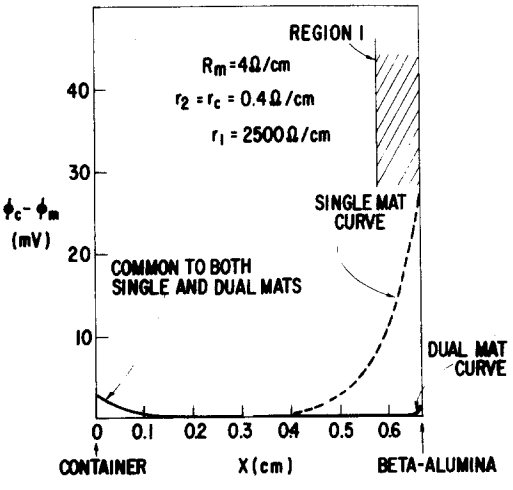

Fig. 5. Reaction rate distribution for dual and single mat geometries ($r_2 = 0{\cdot}4\,\Omega\,cm^{-1}$).

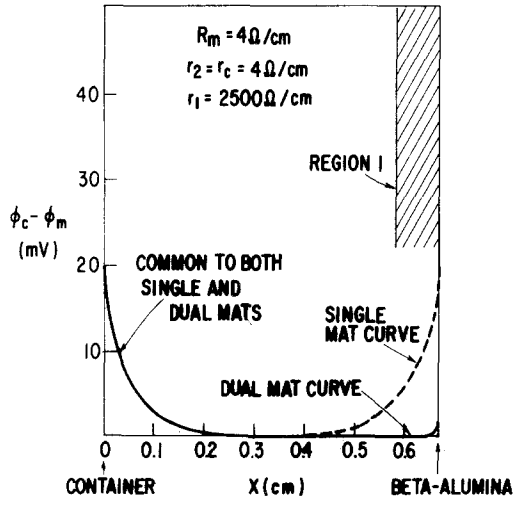

Fig. 6. Reaction rate distribution for dual and single mat geometries ($r_2 = 4{\cdot}0\ \Omega\ cm^{-1}$).

less of carbon mat resistivity. Since the slope resistance is influenced by polysulphide composition [11], it should also be affected by carbon mat resistivity. Assigning a precise value for ρ, however, is extremely difficult [3]. Therefore, the same ρ was used throughout the present analysis. This led to artificially low values of $(\phi_c - \phi_m)$ which should not be confused with a reaction rate approaching zero. In Figs. 5–7, one should consider the relative curve shapes of the reaction rate distribution and not their absolute values.

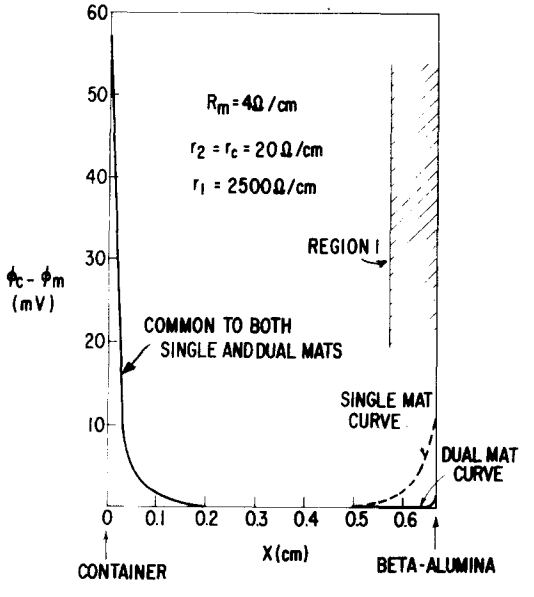

Fig. 7. Reaction rate distribution for dual and single mat geometries ($r_2 = 20\ \Omega\ cm^{-1}$).

The curves indicate that the presence of mat 31 drastically reduces the rate of reaction in the vicinity of the solid electrolyte. This behaviour effectively restricts sulphur formation at the beta-alumina interface and enables greater utilization of the reactants to occur (i.e., operation within the two-phase region). The reaction rate adjacent to the container wall is identical for both geometries but is altered by changing r_2. Region 1 remains essentially independent. Therefore, a low resistance carbon mat (e.g., $r_2 = 0{\cdot}4\ \Omega\ cm^{-1}$) reduces the reaction rate near the container and subsequently leads to a more uniform distribution. In the single mat arrangement this same material predicts a substantial production of sulphur at the beta-alumina interface during charging (Fig. 5).

The decrease in reaction rate for region 1 is obviously due to mat 31. Its high resistance compels all the current to be carried through the melt within this segment, i.e., $J = I_0$. The area underneath the curve verifies this effect. Equation 3 indicates that $(\phi_c - \phi_m)$ is proportional to dI/dx and by integrating this quantity one finds

$$\int \frac{dI}{dx}\,dx = I(x) + C. \tag{23}$$

That is, the area represents a measure of the electronic current within the electrode. In comparing the two configurations it is evident that only the single mat cases have sizeable electronic components in region 1. Thus, the potential distribution model readily explains the effectiveness of the gradated resistance sulphur electrode design. Suppression of the reaction rate at the beta-alumina interface reduces the likelihood for passivating this electrode and allows cells to be routinely charged into the two-phase region.

The performance of laboratory sodium-sulphur cells supports these contentions. Ampere-hour capacities are shown in Fig. 8 for two cells with different sulphur electrode structures. The solid lines represent the extent of cell charge (upper) and discharge (lower); the asterisk marks the position of the two phase sulphur/polysulphide boundary. Specific details of cell testing were described previously [6]. Cell 330 contained the gradated electrode geometry (mat 31 adjacent to the beta-alumina) and consistently cycled into the two-phase region. Cell 277, however, possessed no such layer and only operated in the one-phase

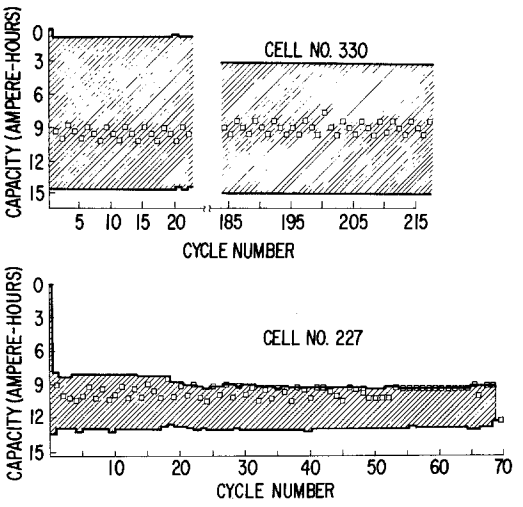

Fig. 8. Capacity performance for cells with and without the gradated resistance sulphur electrode.

zone. These results are totally consistent with the potential distribution model (Fig. 6).

5.2. *Interfacial reactions*

Another implication of the model is the existence of a heterogeneous reaction rate distribution within the sulphur electrode. Certain undesirable, time-dependent cell cycling characteristics may be produced as a result of interfacial reactions. The potential difference $(\phi_c - \phi_m)$ provides information concerning the nature of the electrochemical reactions at the carbon/sodium polysulphide interface when one compares these calculated values with experimental results from voltammetric studies [9–12]. Deviations from linearity are associated with the production of passivating films. Cathodic curves suggest the presence of a sodium polysulphide film, possibly Na_2S_2, while anodic results suggest the formation of elemental sulphur. The potentials where these processes occur are dependent upon composition and temperature but generally fall in the region of $-0{\cdot}35$ V for the cathodic film and $0{\cdot}15$ V for the anodic one in Na_2S_4 at 350° C [9]. A direct, quantitative comparison of $(\phi_c - \phi_m)$ with these potentials is difficult because the calculated $(\phi_c - \phi_m)$ values are uncorrected for their reversible potential. Nonetheless, it is evident that the larger $(\phi_c - \phi_m)$ becomes the greater the probability of film formation. As the melt composition is changed the propensity for polysulphide and sulphur formation are selectively enhanced in Na_2S_3 and Na_2S_5 respectively.

The above discussion indicates the likelihood of film formation at the carbon/sodium polysulphide interface. The presence of these products is capable of explaining the most commonly observed time-dependent cycling behaviour; resistance increase without capacity loss. The formation of a polysulphide film during discharge and a sulphur film during charge would disrupt the contact between the container and carbon fibres and lead to increased cell resistance. This mechanism is consistent with the recent calculations by Gibson [14] who found that cell resistance may indeed increase when electronic and ionic contact resistances are present between the current collector and the carbon matrix. Capacity loss does not have to be appreciable because film formation can be confined to well localized regions at the container wall [15]. Production of sulphur during charge serves to increase cell resistance and accounts for the higher values observed in recent a.c. impedance measurements of cycling cells [16]. Corrosion of the metallic container may also contribute to a time-dependent resistance increase [17]. Larger capacity losses (> 20%) could occur if polysulphide formation advanced continuously from the container to the solid electrolyte. Excessive container corrosion may contribute here as well.

6. Summary

Experimental results indicate that the potential distribution within the carbon matrix is responsible for the improved rechargeability of a new sulphur electrode design. Potential distributions were computed for this design in the one-phase region, following and extending the derivation of Gibson. The resulting model elucidates the role played by the high resistance carbon mat in the gradated sulphur electrode design. Placing the mat adjacent to the beta-alumina electrolyte compels all the current in this region to be carried by the melt. By drastically reducing the electronic current, sulphur formation at the beta-alumina interface is effectively suppressed and the cell readily charges into the two-phase region. In the single mat configuration sulphur production is enhanced and ion transport is impeded.

The model also provides information concerning the types of electrochemical reactions occurring at the carbon/sodium polysulphide interface. Formation of sulphur films on charge and polysulphide ones on discharge are indeed possible and liable to affect long-term cell performance by various mechanisms.

Acknowledgements

This work was supported in part by the Electric Power Research Institute.

References

[1] M. W. Breiter, J. B. Bush, Jr, S. P. Mitoff, O. Muler and W. L. Roth, *Proceedings of Energy Storage Symposium,* The Electrochemical Society, Princeton (1976) p. 165.
[2] S. P. Mitoff, M. W. Breiter and D. Chatterji, *Proceedings of the 12th IECEC,* Vol. 1 Washington, D.C. (1977) p. 359.
[3] J. G. Gibson, *J. Appl. Electrochem.* 4 (1974) 125.
[4] S. A. Weiner, *Proceedings of the Energy Storage Symposium,* The Electrochemical Society, Princeton (1976) p. 141.
[5] J. L. Sudworth, A. R. Tilley and J. M. Bird, *Proceedings of the Load Leveling Symposium,* The Electrochemical Society, Princeton (1977) p. 377.
[6] D. Chatterji, S. P. Mitoff and M. W. Breiter, *ibid* p. 251.
[7] F. A. Ludwig, R. W. Minck and S. A. Weiner, US Patent 3980 496.
[8] R. J. Bones and T. L. Markin, Extended Abstracts, Electrochemical Society Metting, (1977) p. 151.
[9] K. D. South, J. L. Sudworth and J. G. Gibson, *J. Electrochem. Soc.* **119** (1972). 544.
[10] R. D. Armstrong, T. Dickinson and M. Reid, *Electrochim. Acta* **20** (1975) 709.
[11] R. D. Armstrong, T. Dickinson and M. Reid, *ibid* **21** (1976) 935.
[12] R. P. Tischer and F. A. Ludwig, 'Advances in Electrochemistry and Electrochemical Engineering' (edited by H. Gerischer and C. W. Tobias) Vol. 10, John Wiley and Sons, New York (1977) p. 391.
[13] V. S. Daniel-Beck, *Zhur. Fiz. Khim.* **22** (1948) 697.
[14] J. G. Gibson, *International Symposium on Molten Electrolytes and High Temperature Batteries,* Brighton (1977).
[15] R. J. Bones, R. J. Brook and T. L. Markin, 'Power Sources 5' (edited by D. H. Collins) Academic Press, London (1975) p. 539.
[16] M. W. Breiter and B. Dunn, unpublished results.
[17] F. G. R. Zobel, *International Symposium on Molten Electrolytes and High Temperature Batteries,* Brighton (1977).